

# Atomistic Modeling of Charge-Trapping Defects in Amorphous Ge-Sb-Te Phase-Change Memory Materials

Konstantinos Konstantinou\* and Stephen R. Elliott

Understanding the nature of charge-trapping defects in amorphous chalcogenide alloy-based phase-change memory materials is important for tailoring the development of multilevel memory devices with increased data storage density. Herein, hybrid density-functional theory simulations have been employed to investigate electron- and hole-trapping processes in melt-quenched glassy models of four different Ge-Sb-Te compositions, namely, GeTe, Sb<sub>2</sub>Te<sub>3</sub>, GeTe<sub>4</sub>, and Ge<sub>2</sub>Sb<sub>2</sub>Te<sub>5</sub>. The calculations demonstrate that extra electrons and holes are spontaneously trapped, creating charge-trapping centers in the bandgap of the amorphous materials. Over- and undercoordinated atoms, tetrahedral and “see-saw” octahedral-like geometries, fourfold rings, homopolar bonds, near-linear triatomic configurations, and chain-like motifs comprise the range of the defective atomic environments that have been identified in the structural patterns of the charge-trapping sites inside the glassy networks. The results illustrate that charge trapping corresponds to an intrinsic property of the glassy Ge-Sb-Te systems, show the impact of electron and hole localization on the atomic bonding of these materials, and they may have important implications related to the operation of phase-change electronic-memory devices.

computing applications, as well as for new storage-class memory devices.<sup>[2]</sup> The function of phase-change random-access electronic-(optical)-memory (PCRAM) devices is governed by the application of voltage (laser) pulses, which switch the chalcogenide memory material due to Joule heating, very rapidly ( $\approx$ ns) and reversibly, between a degenerate semiconducting, electrically conductive crystalline state (1-bit) and a semiconducting, electrically resistive amorphous (glassy) state (0-bit).<sup>[3]</sup>

The existence of defect-related electronic states in the chalcogenide materials has been considered to be influential in the operation of PCRAM devices.<sup>[4–6]</sup> The resistance contrast between the crystalline and amorphous states has been associated with defects that affect the position of the Fermi level in the two structural phases.<sup>[7,8]</sup> The electric-field-assisted threshold switching in chalcogenide glasses has been attributed to localized states in the bandgap and also to the electron-trapping kinetics associated

with these defect electronic states.<sup>[9–11]</sup> The electrical resistance of the amorphous phase in a PCRAM cell increases (“drifts”) logarithmically with time, hindering the development of multibit storage, multilevel programming in PCRAM devices.<sup>[2]</sup> The time-dependent, resistance-drift phenomenon has been ascribed to structural relaxation of the glassy state,<sup>[12–15]</sup> which is strongly correlated to the annihilation of localized mid-gap defect states from the bandgap of the glass.<sup>[16–21]</sup> The intrinsic charge-trapping processes at the localized electronic states of the amorphous material have also been considered as an alternative (electronic) explanation of the resistance drift.<sup>[22–24]</sup>


Atomistic simulations have reported the existence of several localized unoccupied and occupied electronic states in the vicinity of the bandgap in amorphous phase-change materials. Zipoli et al. associated the localization of defects in the bandgap of models of glassy GeTe with clusters of Ge atoms, in which at least one Ge atom is over- or undercoordinated.<sup>[18]</sup> In some cases, Ge–Ge bonds are present, whereas in some other cases, the Ge atoms are not bonded to each other.<sup>[18]</sup> In addition, GeTe cubes, not properly aligned and sharing a Ge atom, were also identified as possible structural motifs that can host defect states in their model structures.<sup>[18]</sup> Gabardi et al. reported that the mid-gap states in glassy GeTe originate from a kind of Ge–Ge chain-like structure, where most Ge atoms are 4-coordinated in a defective-octahedral geometry.<sup>[17]</sup> Raty et al. correlated the emergence of in-gap states in amorphous GeTe with the Ge–Ge homopolar

## 1. Introduction

Phase-change memory materials based on Ge-Sb-Te alloys encode stored digital binary data as metastable structural states of the chalcogenide material with contrast in optoelectronic properties, and they correspond to a contender for next-generation, nonvolatile electronic-memory technology.<sup>[1]</sup> Moreover, they are also promising candidates for neuromorphic and in-memory

K. Konstantinou  
Computational Physics Laboratory  
Faculty of Engineering and Natural Sciences  
Tampere University  
FI-33014 Tampere, Finland  
E-mail: konstantinos.konstantinou@tuni.fi

S. R. Elliott  
Physical and Theoretical Chemistry Laboratory  
University of Oxford  
Oxford OX1 3QZ, UK

 The ORCID identification number(s) for the author(s) of this article can be found under <https://doi.org/10.1002/pssr.202200496>.

© 2023 The Authors. physica status solidi (RRL) Rapid Research Letters published by Wiley-VCH GmbH. This is an open access article under the terms of the Creative Commons Attribution License, which permits use, distribution and reproduction in any medium, provided the original work is properly cited.

DOI: 10.1002/pssr.202200496

bonds from Ge atoms in tetrahedral configurations.<sup>[16]</sup> Li et al. proposed a valence-alternation Ge–Ge chain model, from overcoordinated Ge atoms, for the mid-gap states in amorphous GeTe.<sup>[25]</sup>

Caravati et al. associated a (rather delocalized) mid-gap state in a fast-quenched amorphous model of Ge<sub>2</sub>Sb<sub>2</sub>Te<sub>5</sub> with Sb–Te chain-structure motifs.<sup>[26]</sup> In our previous work, we demonstrated that 5-coordinated Ge atoms are the dominant local defective bonding environments that are mostly responsible for hosting the mid-gap electronic states in glassy Ge<sub>2</sub>Sb<sub>2</sub>Te<sub>5</sub>.<sup>[27]</sup> The analysis (from an ensemble of 30 model structures) revealed that the mid-gap defect states are spatially localized on complex crystalline-like atomic fragments within the amorphous network, consisting of groups of over- and undercoordinated Ge atoms and fourfold ring structures, while Ge–Ge bonds can be present in the overall geometry of the defect local environment.<sup>[27]</sup> In addition, we demonstrated that electrons can be trapped spontaneously by these mid-gap states, creating deep electron-trap centers in the bandgap of the modeled system.<sup>[27]</sup>

Recently, we also showed that spontaneous electron- and hole-trapping events are energetically favorable at the conduction- and valence-band edges in amorphous Ge<sub>2</sub>Sb<sub>2</sub>Te<sub>5</sub>.<sup>[24]</sup> One-electron traps produce deep occupied states in the bandgap, located in close proximity to the top of the valence band, while one-hole traps lead to the creation of unoccupied states around mid-gap.<sup>[24]</sup> The intrinsic defective-octahedral Ge and Sb sites inside the amorphous Ge<sub>2</sub>Sb<sub>2</sub>Te<sub>5</sub> network have been found to be responsible for the charge trapping.<sup>[24]</sup> The near-linear triatomic Te–Ge/Sb–Te/Ge/Sb environments from the axial bonds in “see-saw” 4-coordinated or 5-coordinated defective-octahedral configurations correspond to the atomic geometries where the extra electrons and holes are trapped.<sup>[24]</sup> In addition, five-membered chain-like structural motifs, comprised of two connected triads, have also been identified as potential charge-trapping sites.<sup>[24]</sup>

Understanding charge-trapping processes at the localized defect electronic states of the glassy state is of great importance with respect to the operational conditions in PCRAM devices. In this study, we aim to extend our previous work by performing electron- and hole-trapping calculations for amorphous models of the two binary end-members of the Ge-Sb-Te compositional tie-line, namely, GeTe and Sb<sub>2</sub>Te<sub>3</sub>, the eutectic composition GeTe<sub>4</sub>, and for a 900-atom model of the canonical ternary Ge<sub>2</sub>Sb<sub>2</sub>Te<sub>5</sub> composition. In this way, and through the compositional diversity of the investigated models, we envisage a range of intrinsic charge-trapping centers in these chalcogenide glassy materials, and we identify several potential structural patterns for electron-/hole-trapping sites inside the amorphous structure of phase-change memory materials.

## 2. GeTe

An 180-atom structural model of amorphous GeTe, generated by ab initio (DFT) molecular dynamics (MD) simulations in previous work,<sup>[28]</sup> was used to investigate the electronic structure of this binary composition in this study. The total and partial electronic densities of states (DOS and PDOS, respectively) near the top of the valence band and the bottom of the conduction band of the glassy GeTe model are shown in **Figure 1**. A hybrid-DFT electronic-structure calculation results in a Kohn–Sham (KS)

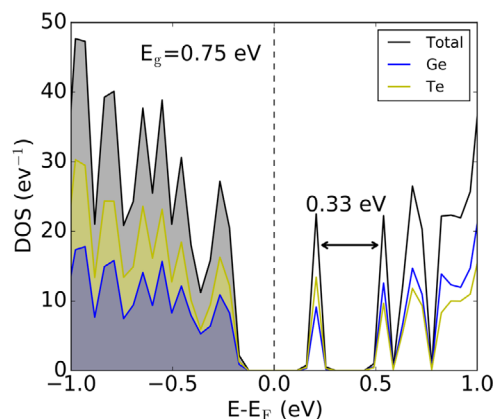


**Figure 1.** Total and partial electronic densities of states (DOS/PDOS) near the top of the valence band and the bottom of the conduction band of the amorphous GeTe model.

bandgap,  $E_g$ , of 0.75 eV for the relaxed ground state, which agrees very well with the experimentally reported values for glassy GeTe ( $E_g = 0.80$  eV,<sup>[29]</sup> 0.81 eV<sup>[5,30]</sup>). A well-defined unoccupied electronic state emerges inside the bandgap, which is located at an energy level of 0.33 eV below the conduction-band edge. This in-gap state is dominated by the contribution from Te-atom states, with some contribution from Ge-atom states as well (Figure S1, Supporting Information, shows the molecular orbital associated with the in-gap state). In contrast, for the conduction-band-minimum state, the contribution from Ge-atom states is more significant compared to that from Te atoms, suggesting a different character of electron localization between the two electronic states.

An extra electron was added to the relaxed ground state of the amorphous model and the geometry of the system was then reoptimized. The DOS and PDOS of the simulated glass with the trapped electron are shown in Figure S2, Supporting Information. The in-gap defect state present in the neutral GeTe glass captures the extra electron and becomes an occupied state. The position of the KS level for the electron trap is 0.58 eV below the bottom of the conduction band, hence indicating a relatively deep trap in the electronic structure of the glassy model. An analysis of the spin-density distribution for the modeled system with the extra electron, as shown in **Figure 2a**, reveals the structural motifs that host the additional charge inside the glassy network. The extra electron is (partially) localized among a group of Ge atoms within the amorphous structure. The individual, characteristic contributions related to the structural pattern of the electron trap can be distinguished as follows: a) a Te–Ge–Te triatomic environment with a near-linear bond angle of 163.4° from a 4-coordinated Ge atom in a “see-saw” configuration; b) a Ge–Te–Ge–Te fourfold ring structure created from two 4-coordinated Ge atoms; c) a 5-coordinated Ge atom connected to a tetrahedral Ge atom through a Ge–Ge bond; and d) two defective octahedral Ge sites (one 5-coordinated and one “see-saw” 4-coordinated) and a 3-coordinated Ge atom with a significant presence of Ge–Ge bonds in their geometries.

The nature of electron spatial localization for the conduction-band-edge state in the amorphous GeTe model can be examined

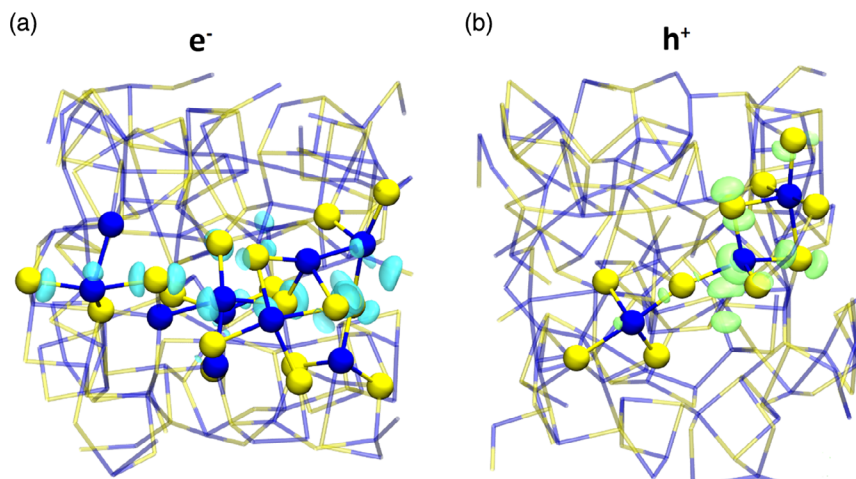


**Figure 2.** Spin-density distribution of the extra: a) trapped electron ( $e^-$ ); and b) trapped hole ( $h^+$ ) in the GeTe glass model, together with the atomic configurations of the respective charge-trapping environments inside the glassy structure. Ge atoms are blue and Te are yellow. The bonds in the rest of the amorphous network are rendered as sticks, colored according to the type of atoms involved in the bonding. In both configurations, the isovalue of the spin density (cyan isosurface for  $e^-$ ; green isosurface for  $h^+$ ) is equal to  $0.0015 \text{ e } \text{\AA}^{-3}$ .

by visualization of the molecular orbital of the electronic state, as shown in **Figure 3**. Five Ge atoms are connected to each other, forming a continuous chain-like motif that participates in the partial spatial localization of the electronic state at the bottom of the conduction band, revealing a different defective atomic geometry than the electron-trap defect associated with the mid-gap state of the glassy model.

An extra hole added to the neutral amorphous GeTe geometry will be potentially localized at the top of the valence band in the highest occupied molecular orbital (HOMO) of the simulated structure. A hybrid-DFT calculation showed that hole trapping

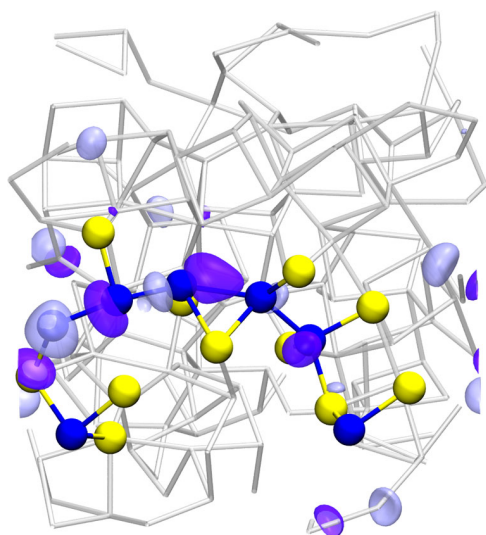


**Figure 3.** Molecular orbital of the conduction-band-minimum electronic state in the amorphous GeTe model. Ge atoms are blue and Te are yellow. The atomic bonds in the rest of the amorphous network are rendered in gray. The purple and light blue isosurfaces depict the molecular-orbital wave function amplitude of the electronic state, and are plotted with isovalues of  $+0.025$  and  $-0.025 \text{ e } \text{\AA}^{-3}$ , respectively.

produces an unoccupied state in the bandgap of the glassy model, located at a KS level of  $0.27 \text{ eV}$  above the valence-band maximum. The spin-density distribution of the intrinsic hole trap in the GeTe model, as shown in **Figure 2b**, indicates a strong preference for hole localization at defective octahedral sites within the glassy network. Two connected near-linear Te–Ge–Te triatomic environments, with bond angles  $176.1^\circ$  and  $154.9^\circ$ , associated with two different “see-saw” 4-coordinated Ge atoms, form a chain-like structure where the hole is trapped. In addition, a Te–Ge–Te triad with a wide,  $167.3^\circ$ , angle from a 5-coordinated Ge atom in a square-pyramidal configuration and a fourfold ring structure participate in the hole-trap environment.

We note that Longeaud et al.<sup>[4]</sup> reported experimental results showing two defect states in the bandgap of amorphous GeTe, located at energy levels of  $0.41$  and  $0.37 \text{ eV}$  (above the top of the valence band), respectively, while these (monovalent) defects will become negatively charged when occupied with an electron (i.e., acceptor-like electronic states). Additionally, they also identified a defect state at an energy level of  $0.26 \text{ eV}$  in the bandgap of the chalcogenide structure, which can act as a donor-like state (i.e., positively charged when occupied with a hole).<sup>[4]</sup> In this study, the hybrid-DFT electronic-structure calculations manifested a discrete in-gap electronic state located at an energy level of  $0.42 \text{ eV}$  above the top of the valence band of the glassy GeTe model, which can capture extra electrons. Moreover, hole trapping (positively charged system) produced a new electronic state in the bandgap of the amorphous model, located at a KS level of  $0.27 \text{ eV}$  above the valence-band maximum.

### 3. $\text{Sb}_2\text{Te}_3$

In our recent work, an amorphous 250-atom  $\text{Sb}_2\text{Te}_3$  model was generated using DFT-MD simulations and by following a melt-and-quench approach.<sup>[31]</sup> The atomic geometry of the glassy model was further optimized by employing a hybrid-DFT calculation. The electronic-structure calculation resulted in

$E_g = 0.75$  eV for the relaxed ground state, devoid of defect-related in-gap electronic states.<sup>[31]</sup> This computed value of the bandgap is in agreement with the value that had been previously reported by a different DFT-MD modeling study of glassy  $\text{Sb}_2\text{Te}_3$  ( $E_g = 0.69$  eV),<sup>[32]</sup> as well as with the experimentally reported values ( $E_g = 0.52$  eV,<sup>[29]</sup> 0.55–0.8 eV<sup>[33]</sup>). An analysis of the PDOS around the Fermi level of the simulated amorphous structure showed that both Sb-atom and Te-atom states contribute to the electronic states at the band edges.<sup>[34]</sup>

In this study, an electron-trapping event was modeled by injecting an extra electron in the relaxed neutral geometry of the  $\text{Sb}_2\text{Te}_3$  model, and then minimizing the energy of the system with respect to its atomic coordinates. The extra electron added to the glass model occupies the lowest unoccupied molecular orbital (LUMO; see Figure 1 in Ref. [34]) at the bottom of the conduction band. The DOS and PDOS of the simulated glass with the trapped electron are shown in Figure 4a. The hybrid-DFT optimization shows that the position of the electron-trap state is 0.55 eV below the conduction-band edge. We note that a similar calculation for a hole-trapping event showed that the extra hole was not trapped in this model of amorphous  $\text{Sb}_2\text{Te}_3$ . However, an examination of an ensemble of glassy structures would be necessary to gain a statistical understanding of the prevalence of possible hole localization in this binary system.

Figure 4b illustrates the spin-density distribution and the atomic geometry of the electron trap identified in the glassy  $\text{Sb}_2\text{Te}_3$  model. The extra electron is localized rather weakly within the amorphous network; nevertheless, there are some interesting observations related to the structural pattern that hosts the electron trap: 1) a Te–Sb–Sb near-linear triatomic environment, from a 5-coordinated Sb atom, with an angle of 155.9°; 2) a significant presence of Sb–Sb homopolar bonds; 3) three Sb atoms (from three different defective-octahedral configurations) connected to each other, forming a three-member chain-like motif (Sb–Sb–Sb angle = 144.1°); 4) a 4-coordinated Sb atom bonded only to other Sb atoms; 5) a 3-coordinated Sb atom in a trigonal-pyramidal configuration; 6) 2-coordinated Sb atoms; and 7) three distorted fourfold ring structures connected to each other.

Double-charge trapping was investigated in the amorphous model of  $\text{Sb}_2\text{Te}_3$  by adding a second electron to the existing single-electron trapped simulated structure and then reoptimizing its geometry. We note that when the first excess electron was added to the neutral system, it occupied the alpha-spin channel (spin up, +1/2) of the LUMO state, while the second extra electron will occupy the beta-spin channel (spin down, –1/2) of this electronic state. It was found that the addition of the second electron facilitates the creation of a much deeper singlet-occupied KS state in the bandgap of the glassy model compared to the one-electron trap, located at 0.73 eV below the bottom of the conduction band (see Figure S3, Supporting Information, for a comparison between the electronic densities of states with one and two extra trapped electrons in the glassy  $\text{Sb}_2\text{Te}_3$  model).

The hybrid-DFT electronic-structure calculation showed that the second extra electron, even though it is partially localized in the simulated periodic cell, induces atomic relaxations in the structural pattern hosting the one-electron trap leading to structural modifications of local environments in the vicinity of the defect state. This is highlighted in Figure 5a,b, where the addition of the second electron and the subsequent (partial) localization on the same structural site as the first electron leads to bond breaking in the 3-Sb chain-like environment (Sb–Sb interatomic distance = 3.42/3.66 Å for one/two electrons, denoted with a green arrow). In addition, stretching (and hence potential breaking) of a long Sb–Te bond (Sb–Te interatomic distance = 3.47/3.52 Å for one/two electrons) from the 5-coordinated Sb atom in the atomic geometry of the trap was observed, which also leads to breaking of the connected fourfold ring structures (denoted with a blue arrow). Consequently, the induced atomic relaxations caused a lowering in the coordination of the defective-octahedral Sb sites, since the 5-coordinated and the two 4-coordinated Sb atoms become 4- and 3-coordinated, respectively. We note that, in this analysis, bond formation is considered to occur between two nearby atoms as long as the interatomic distance between these atoms is shorter than or equal to 3.5 Å.

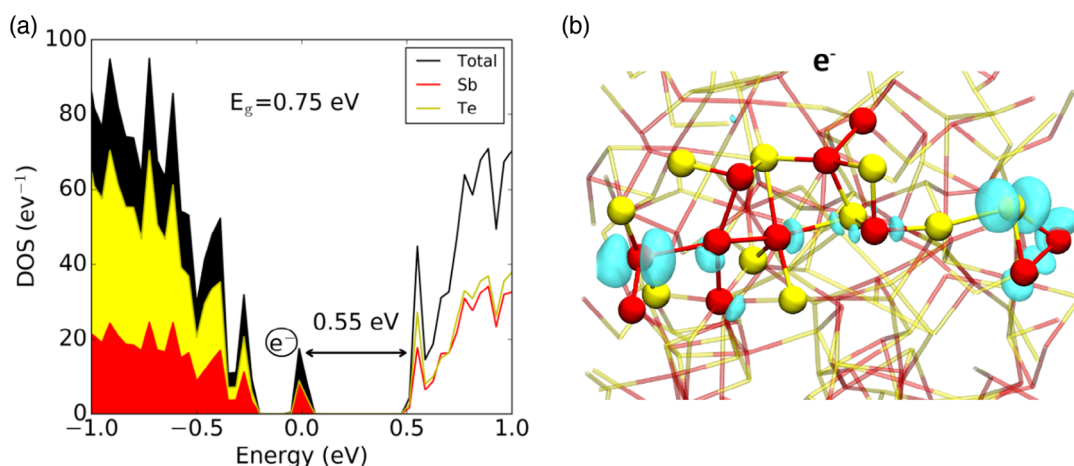


**Figure 4.** a) Total and partial electronic densities of states (DOS/PDOS) near the top of the valence band and the bottom of the conduction band of the amorphous  $\text{Sb}_2\text{Te}_3$  model with a trapped electron ( $e^-$ ). b) Spin-density distribution of the extra  $e^-$ , together with the atomic configuration where the  $e^-$  is trapped inside the glassy structure. Sb atoms are red and Te are yellow. The isovalue of the spin density (cyan isosurface) is equal to  $0.0015 \text{ e} \text{ \AA}^{-3}$ .

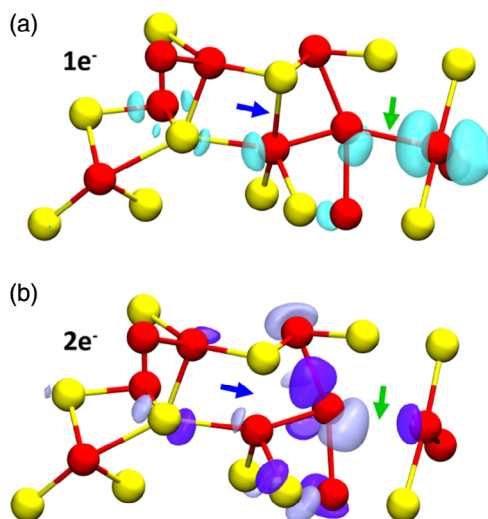


**Figure 5.** a) Spin-density distribution and atomic geometry of the one-electron trapped state ( $1e^-$ ) in the  $Sb_2Te_3$  glass model. The isovalue of the spin density (cyan isosurface) is equal to  $0.0015 e \text{ \AA}^{-3}$ . b) Configuration of the two-electron trapped state ( $2e^-$ ) in the same amorphous model. The colored isosurfaces correspond to the molecular-orbital wave function amplitude of the occupied Kohn-Sham state of the double-electron system, with isovalues equal to  $+0.015 e \text{ \AA}^{-3}$  (purple) and  $-0.015 e \text{ \AA}^{-3}$  (light blue). In both cases, Sb atoms are red and Te are yellow. The blue and green arrows indicate the Sb–Te and Sb–Sb bonds, respectively, that are affected by the localization of the second trapped electron.

#### 4. $Ge_2Sb_2Te_5$

The machine-learned Gaussian Approximation Potential (GAP) developed for Ge–Sb–Te materials<sup>[35]</sup> was employed to generate a periodic amorphous 900-atom  $Ge_2Sb_2Te_5$  model, using classical MD simulations and by following a melt-and-quench approach.<sup>[27]</sup> A hybrid-DFT geometry-optimization calculation for this simulated structure showed a bandgap of 0.63 eV for

the relaxed ground state, while several localized unoccupied in-gap states were identified in the electronic structure of this large glassy model.<sup>[27]</sup> The lowest (deepest) in-gap electronic state is located at an energy level of 0.37 eV below the conduction-band edge, while the next two in-gap states in the DOS of the model structure are placed at 0.14 and 0.19 eV above the deepest defect state.<sup>[27]</sup> By using a threshold criterion (0.02), based on the calculated inverse participation ratio (IPR) values, for the degree of spatial localization of each single-particle KS state in the electronic structure of this 900-atom glassy model,<sup>[27]</sup> 13 localized defect electronic states were counted, leading to an estimated defect density of  $0.45 \times 10^{21} \text{ cm}^{-3}$ , which is in reasonably good agreement with the experimentally reported values for defects in amorphous  $Ge_2Sb_2Te_5$  ( $3.9 \times 10^{21} \text{ cm}^{-3}$  and  $5 \times 10^{21} \text{ cm}^{-3}$ ).<sup>[6]</sup> See the Supporting Information for a more extensive comment about the defect-density estimations that can be obtained from atomistic glassy models.

In this study, an extra electron was added to the relaxed ground state of the 900-atom amorphous model, and the geometry of the system was then reoptimized with a hybrid-DFT calculation. The deepest in-gap defect state, present in the neutral glass, captures the extra electron and becomes an occupied state. The electron-trap center is located at 0.12 eV above the top of the valence band, corresponding to a deep trap in the bandgap of the glassy material. An analysis of the spin-density distribution for the electron trap, as shown in **Figure 6a**, reveals that the extra electron is strongly spatially localized inside the amorphous network. The atomic environment that hosts the electron-trap defect state, as shown in **Figure 6b**, is comprised of two Ge atoms, one 6-coordinated and another 4-coordinated in a tetrahedral geometry, which are bonded to each other. The three features associated with the configuration of the electron trap (overcoordinated Ge atom, tetrahedral Ge atom, and Ge–Ge bond) are characteristic environments related to localized gap states that have been identified in models of amorphous  $Ge_2Sb_2Te_5$  and GeTe phase-change memory materials.<sup>[16–19,21,25,27]</sup>

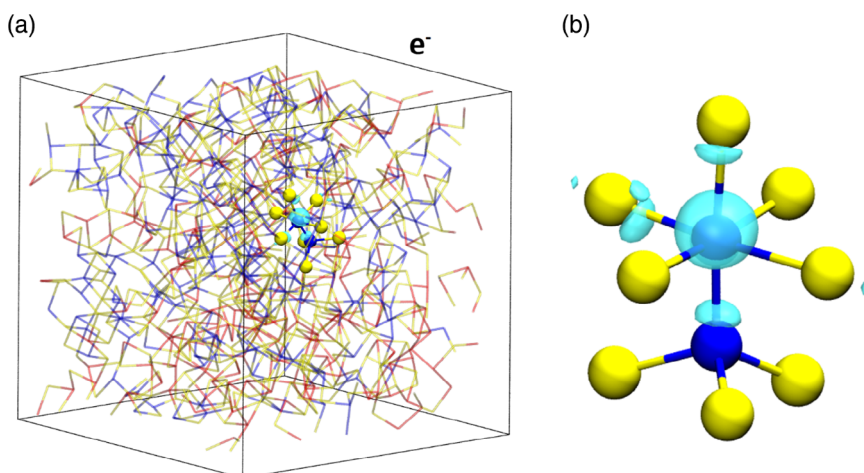


**Figure 6.** a) Spin-density distribution of the trapped electron ( $e^-$ ) in the 900-atom  $Ge_2Sb_2Te_5$  amorphous model. b) Atomic environment where the extra  $e^-$  is (well) localized inside the glassy structure. Ge atoms are blue, Sb are red, and Te are yellow. The bonds in the rest of the amorphous network are rendered as sticks, colored according to the type of atoms involved in the bonding. The isovalue of the spin density (cyan isosurface) is equal to  $0.002 e \text{ \AA}^{-3}$ .

Our previous calculations for an ensemble of 30 models of glassy  $\text{Ge}_2\text{Sb}_2\text{Te}_5$ , each containing 315 atoms, demonstrated that spontaneous electron-trapping events, either at the mid-gap states or at the LUMO of these model structures, lead to the creation of deep-trap states, located in close proximity to the top of the valence band.<sup>[24,27]</sup> When the extra electron occupies one of the mid-gap electronic states, it is localized among a group of overcoordinated Ge atoms inside the glass structure.<sup>[27]</sup> However, the spatial localization of this electron center is more extended compared to the strongly localized character of the electron trap identified here for the 900-atom  $\text{Ge}_2\text{Sb}_2\text{Te}_5$  model, revealing a possible system-size effect. When the extra electron is trapped at the conduction-band-edge electronic states of these glassy models, it is localized on near-linear triatomic environments (mostly) from defective octahedral-like “see-saw” geometries, which can also be connected to each other, creating chain-like electron-trapping configurations.<sup>[24]</sup>

Hole localization at the top of the valence band of the 900-atom model structure was investigated with a hybrid-DFT calculation. It was found that hole trapping produces an unoccupied state in the bandgap of the glassy model located at 0.27 eV above the valence-band maximum, corresponding to a KS state around mid-gap, and also very close to one of the other unoccupied in-gap defect states originally present in the simulated  $\text{Ge}_2\text{Sb}_2\text{Te}_5$  structure. The HOMO in the neutral geometry of the amorphous model, as shown in Figure 7a, is partially localized on two Ge atoms, which are not bonded to each other. The first Ge atom ( $\text{Ge}_1$ ) is 4-coordinated in a “see-saw” defective-octahedral configuration, where the spatial localization of the electronic state occurs on a distinct triatomic Te–Ge–Te environment with a wide (almost linear) angle of  $176^\circ$ , while the second Ge atom ( $\text{Ge}_2$ ) is 3-coordinated in a trigonal-pyramidal configuration. The spin-density distribution of the hole trap in this glassy

model of  $\text{Ge}_2\text{Sb}_2\text{Te}_5$  is shown in Figure 7b. Hole localization results in bond switching between the two Ge atoms. Upon hole trapping and following geometry relaxation, the  $\text{Ge}_1$  atom becomes 3-coordinated due to the breaking of one of the long, axial Ge–Te bonds, while a new bond is formed in the neighboring atomic environment of  $\text{Ge}_2$  with the same Te atom (shown in the black dashed frame), making it 4-coordinated (tetrahedral). Here, bond formation is considered to occur between two nearby atoms as long as the interatomic distance between these atoms is shorter than or equal to  $3.2 \text{ \AA}$ .

In our recent work, we showed that the involvement of the intrinsic wide angle (near-linear) Te–Ge/Sb–Te triatomic environments from the defective octahedral-like (“see-saw” 4-coordinated and 5-coordinated) configurations is instrumental in the hole-trapping processes at the top of the valence band in amorphous models of  $\text{Ge}_2\text{Sb}_2\text{Te}_5$  (315 atoms).<sup>[24]</sup> Also, we observed hole (and electron) localization to occur in such near-linear triads where the one-end Te (or Ge/Sb) atom is nonbonded.<sup>[24]</sup> Moreover, we demonstrated that, after electron/hole injection, the localization of the extra charge that is trapped in these atomic environments causes bond stretching (i.e., weakening) for some of these axial (long) bonds, hence, reducing the energy barrier for breaking one such Ge/Sb–Te bond.<sup>[24]</sup> The bond switching observed in the hole-trapping event in the  $\text{Ge}_2\text{Sb}_2\text{Te}_5$  glassy model studied here does not necessarily need to occur in order for these configurations to act as electron/hole traps inside the chalcogenide structure, since this will depend on the degree of atomic relaxation (atomic displacements) upon geometry optimization of the modeled structure, following electron/hole injection, as well as on the vicinity of the host-trapping atomic environment. In addition, very recently, we also demonstrated that the application of a sufficiently high external electric field induces atomic relaxations of the amorphous structure,

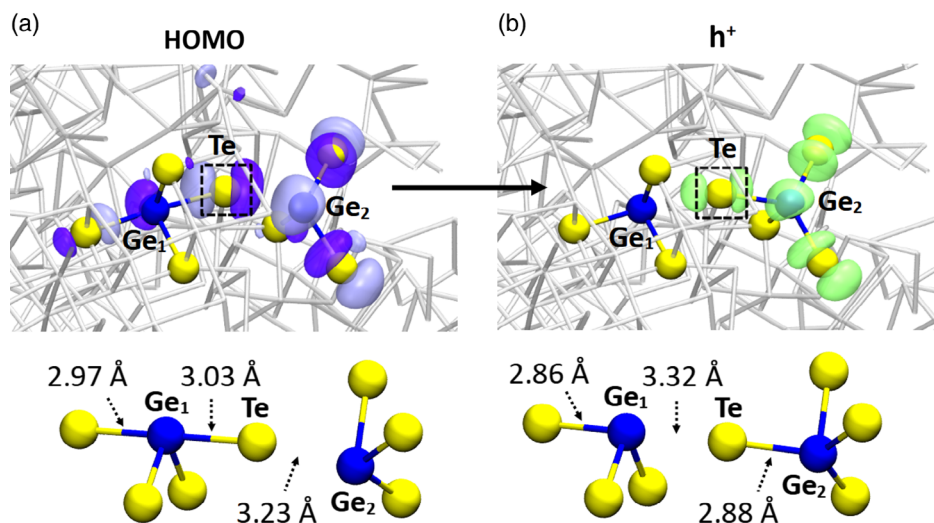


**Figure 7.** a) Molecular orbital of the valence-band-maximum electronic state (HOMO) in the 900-atom  $\text{Ge}_2\text{Sb}_2\text{Te}_5$  glassy model. The purple and light blue isosurfaces depict the molecular-orbital wave function amplitude of the electronic state, and are plotted with isovalues of  $+0.02$  and  $-0.02 \text{ e \AA}^{-3}$ , respectively. b) Spin-density distribution and atomic geometry of the extra trapped hole ( $h^+$ ) in the same amorphous model. The isovalue of the spin density (green isosurface) is equal to  $0.002 \text{ e \AA}^{-3}$ . In both configurations, Ge atoms are blue and Te are yellow. The atomic bonds in the rest of the amorphous network are rendered in gray. The bond lengths indicated by arrows show that hole localization causes significant atomic relaxation in the vicinity of the defect.

resulting in breaking of the weak, polarizable bonds in 5-coordinated Ge atoms, associated with defect-related localized states in glassy  $\text{Ge}_2\text{Sb}_2\text{Te}_5$ .<sup>[21]</sup>

The other two (shallower) in-gap unoccupied states identified in the 900-atom  $\text{Ge}_2\text{Sb}_2\text{Te}_5$  glassy model can also serve as charge-trapping centers. The potential electron-trapping sites associated with these spatially localized electronic states can be examined by visualization of their molecular orbitals. The atomic environment responsible for the spatial localization of the defect electronic state located at 0.23 eV below the bottom of the conduction band is shown in Figure S4, Supporting Information. Two tetrahedral Ge atoms with a Ge–Ge bond in their configurations, one overcoordinated (sixfold) and one undercoordinated (threefold) Ge atom, and two “see-saw” 4-coordinated Ge and Sb atoms create the complex local atomic environment in which the defect state is hosted inside the simulated structure. Moreover, a square Ge–Te–Sb–Te ring is formed in the vicinity of the two defective-octahedral sites of Ge and Sb atoms. A group of four Ge atoms is involved in the spatial localization of the electronic state located at 0.18 eV below the conduction-band edge, shown in Figure S5, Supporting Information. More specifically, one 5-coordinated, one 3-coordinated, one 4-coordinated in a “see-saw” configuration, and one 4-coordinated in an (almost) tetrahedral geometry participate in the host structural pattern of the defect state. In addition, the formation of one square and two distorted Ge–Te–Ge–Te connected rings can be observed. It is noted that fourfold rings have been previously identified as an essential feature of the amorphous structure of  $\text{Ge}_2\text{Sb}_2\text{Te}_5$ .<sup>[36,37]</sup>

A defect state at the conduction-band tail in the electronic structure of amorphous  $\text{Ge}_2\text{Sb}_2\text{Te}_5$  has been reported experimentally,<sup>[6]</sup> located at an energy level of 0.39 eV (above the top of the valence band), which is an acceptor-like state (i.e., negatively charged when occupied with an electron). Also, a donor-like defect state (i.e., positively charged when occupied with a hole) at an energy level of 0.25 eV in the bandgap was reported,<sup>[6]</sup> which belongs to the valence band tail. Our hybrid-DFT electronic-structure calculations identified three distinct localized electronic states in the bandgap of the neutral  $\text{Ge}_2\text{Sb}_2\text{Te}_5$

glassy model, located at energy levels of 0.26, 0.40, and 0.45 eV above the valence-band maximum, respectively, which can be viewed as part of the conduction-band tail, and, in principle, they can act as electron-trap hosts. In addition, hole trapping (positively charged system) led to the creation of a defect electronic state in the bandgap of the amorphous model at an energy level of 0.27 eV above the valence-band maximum.

## 5. $\text{GeTe}_4$

Previously, an amorphous structure of 315 atoms of the eutectic  $\text{GeTe}_4$  composition was generated with melt-and-quench DFT-MD simulations.<sup>[38]</sup> In this study, a KS bandgap  $E_g = 0.79$  eV was obtained for the relaxed ground state of this glassy model from a hybrid-DFT geometry-optimization electronic-structure calculation, which agrees very well with the experimentally reported values for amorphous  $\text{GeTe}_4$ , ranging between 0.86 and 0.93 eV.<sup>[39]</sup> The DOS and PDOS near the top of the valence band and the bottom of the conduction band are shown in Figure S6, Supporting Information. No in-gap states were observed in the electronic structure, while both band edges are dominated by Te-atom *p*-states, with some contribution from Ge-atom states as well.

Subsequently, an extra electron ( $e^-$ ) was added to the relaxed neutral ground state of the amorphous  $\text{GeTe}_4$  model and the geometry of the glassy structure was then reoptimized with a hybrid-DFT calculation. The LUMO electronic state, at the bottom of the conduction band, becomes an occupied molecular orbital, and the energy position of this state is 0.45 eV below the conduction-band minimum, indicating a shallower electron-trap state compared to those identified in the other chalcogenide glasses studied here. Correspondingly, the addition of an extra hole ( $h^+$ ) in the relaxed ground state of the neutral system results, following a geometry relaxation, in the production of an unoccupied electronic state, located at an energy level of 0.55 eV above the valence-band maximum, bringing this defect state rather higher than mid-gap.

An analysis of the spin-density distribution for the modeled system with an extra electron, as shown in Figure 8a, reveals that

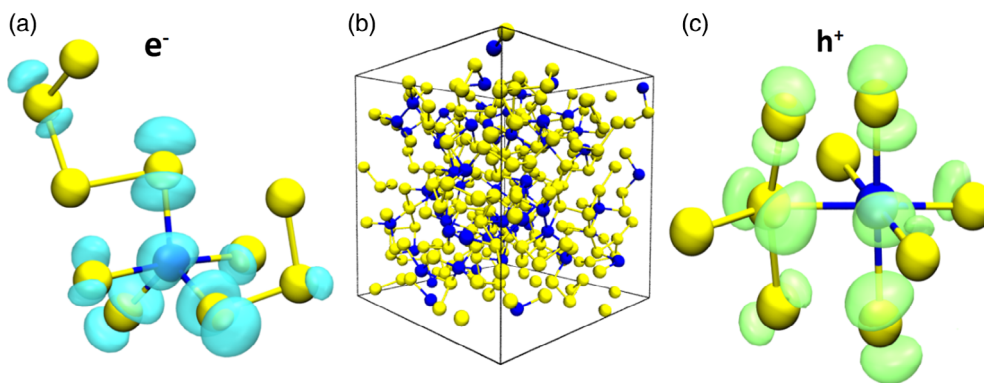


**Figure 8.** a) Spin-density distribution of the trapped electron ( $e^-$ ) in the  $\text{GeTe}_4$  glass model, together with the atomic environment where the extra  $e^-$  is (well) localized inside the glassy structure. The isovalue of the spin density (cyan isosurface) is equal to  $0.0015 \text{ e} \text{ \AA}^{-3}$ . b) Atomistic structure of the 315-atom glassy  $\text{GeTe}_4$  model. c) Spin-density distribution of the trapped hole ( $h^+$ ) in the same amorphous model, together with the configuration where the extra  $h^+$  is (well) localized inside the glassy structure. The isovalue of the spin density (green isosurface) is equal to  $0.0015 \text{ e} \text{ \AA}^{-3}$ . In every configuration, Ge atoms are blue and Te are yellow.

a 5-coordinated Ge atom corresponds to the defective atomic environment where the spatial localization of the electron trap occurs in the simulated glassy structure of GeTe<sub>4</sub> (Figure 8b). In addition, two 2-coordinated Te atoms, bonded only to other Te atoms, participate in the structural pattern responsible for the charge trapping. The spin-density distribution and the atomic geometry of the hole trap are shown in Figure 8c. Hole trapping was found to occur in a configuration where a 6-coordinated Ge atom is connected to a 4-coordinated Te atom. The Te–Ge–Te triad, that is, the link between the two different atomic environments has a pronounced wide angle character, with the calculated angle being 159.7°. The angle of the Te–Te–Te triad that participates in the hole localization is 162.1°, while the Te–Ge–Te triad, solely associated with the Ge atom, has an almost-linear angle of 173°.

We note that the electron-/hole-trapping calculations performed here for the GeTe<sub>4</sub> model highlight that the overcoordinated Ge atoms play a significant role in the charge-trapping events inside the Te-rich glassy structure of this chalcogenide composition.

## 6. Discussion and Conclusion

We report on the results of hybrid-DFT calculations of electron and hole injection, and subsequent trapping, in melt-quenched glassy models of the phase-change memory materials GeTe and Sb<sub>2</sub>Te<sub>3</sub> (the two binary end-members of the Ge-Sb-Te compositional tie-line), Ge<sub>2</sub>Sb<sub>2</sub>Te<sub>5</sub> (the canonical ternary composition), and GeTe<sub>4</sub> (the eutectic composition).

In our previous recent work, we presented a statistical study about electron/hole trapping in many glassy models of Ge<sub>2</sub>Sb<sub>2</sub>Te<sub>5</sub>.<sup>[24]</sup> Here, we expanded the compositional diversity of the investigated models, by exploring charge-trapping processes in three more chalcogenide simulated structures (GeTe, Sb<sub>2</sub>Te<sub>3</sub>, and GeTe<sub>4</sub>). Moreover, we present calculations at the same level of accuracy (hybrid-DFT) for the investigation of charge-trapping defects in a 900-atom Ge<sub>2</sub>Sb<sub>2</sub>Te<sub>5</sub> amorphous model, trying to push the boundaries of the system size (from 315 atoms previously).

The calculations demonstrate that in-gap defect-related unoccupied electronic states in amorphous GeTe and Ge<sub>2</sub>Sb<sub>2</sub>Te<sub>5</sub> can capture extra electrons, leading to the creation of deep electron centers in the bandgap of the glassy materials. Similarly, deep electron-trap states were also identified in the Sb<sub>2</sub>Te<sub>3</sub> and GeTe<sub>4</sub> amorphous models, where electron trapping occurs at the localized states at the bottom of the conduction band. Hole trapping at the top of the valence band leads to the formation of occupied states around mid-gap in the glassy chalcogenide materials.

The energy levels of the defect-electronic states identified in the amorphous Ge<sub>2</sub>Sb<sub>2</sub>Te<sub>5</sub> and GeTe models studied here are in good agreement with the experimentally reported values, while also the system size of the glassy Ge<sub>2</sub>Sb<sub>2</sub>Te<sub>5</sub> simulated structure (900 atoms) provides a credible defect-density estimation compared to experimental measurements. However, we note that in our models, we do not discuss the concept of band tails as such (i.e., the onset of the conduction and valence bands) like they do in experiments, but, instead, we highlight distinct

defect-localized electronic states, either inside the bandgap or at the band edges (top/bottom) of the modeled structures, which can act as potential hosts for the production of electron-/hole-trapping centers. This is also due to the fact that we perform ground-state, spin-polarized DFT calculations, accessing specific electronic states in the electronic structure of the glassy models. In addition, we note that when the extra electrons (holes) occupy the relevant electronic states of the neutral systems, these states are shifted toward the valence-(conduction-)band maximum (minimum) following geometry relaxation. This approach gives us the opportunity to quantify the energy levels of the charge-trapping centers in the bandgap, as well as to study effectively the localization properties of the extra trapped charges inside the simulated structures, information that cannot be obtained experimentally.

The prevailing feature among the four different compositions studied here is that excess electrons and holes are spontaneously trapped in the narrow bandgap of the chalcogenide glassy structures. A difference was observed in the degree of spatial localization for the extra charges inside the amorphous models, since the electron/hole localization was found to be stronger in the Ge<sub>2</sub>Sb<sub>2</sub>Te<sub>5</sub> and GeTe<sub>4</sub> models, whereas a weaker (and more extended) spatial localization was observed within the glassy networks of the GeTe and Sb<sub>2</sub>Te<sub>3</sub> models. Of course, this might be related to size effects and calculations for larger model structures would offer a better quantitative description of the localization properties.

Characteristic atomic environments that are involved in the structural patterns of the electron- and hole-trapping sites are: 1) 4-coordinated Ge and Sb atoms in a “see-saw” defective-octahedral configuration; 2) overcoordinated (5- and 6-coordinated) Ge atoms; 3) tetrahedral Ge atoms with a Ge–Ge bond present in their geometry; 4) square and distorted fourfold ring structures; 5) near-linear triatomic environments from octahedral-like sites; 6) homopolar bonds (Te–Te, Sb–Sb, and Ge–Ge); and 7) 3-coordinated Ge and Sb atoms, and 2-coordinated Te atoms. In addition, Ge–Ge chain-like structures have also been identified as potential electron-trapping sites at the conduction-band edge of the GeTe model.

A structural pattern comprised of an overcoordinated Ge atom connected to a tetrahedral Ge atom through a Ge–Ge bond emerges only when electron trapping is associated with in-gap defect electronic states (in the glassy GeTe and Ge<sub>2</sub>Sb<sub>2</sub>Te<sub>5</sub> models), whereas it (a similar concept) does not appear for the electron-trap environments that are associated with conduction-band-edge localized states (in the glassy Sb<sub>2</sub>Te<sub>3</sub> and GeTe<sub>4</sub> models studied here, as well as in the Ge<sub>2</sub>Sb<sub>2</sub>Te<sub>5</sub> models studied before<sup>[24]</sup>). A predominant common host structural motif in all four compositions is associated with Ge and Sb atoms being in a crystalline-like environment within the amorphous network (in “see-saw” 4-coordinated, square-pyramidal 5-coordinated, and 6-coordinated configurations), and the triatomic, almost-linear environments from these distorted octahedral-like atomic geometries, a view that is in agreement with our previous studies.<sup>[21,24,27]</sup>

A major electronic-related attribute of the axial, long bonds from the near-linear arrangements of triatomic configurations in the defective octahedral-like sites is their large polarizability, which increases the strength of attractive interactions.



These electron-polarized, near-linear atomic motifs of chemically ordered triads provide a broad source of potential charge-trapping sites in the amorphous chalcogenide structures. Electron/hole trapping is facilitated by the high polarizability of the lone-pair orbitals and the marked flexibility (softness) of these precursor structural units, and the subsequent relaxation of their local atomic environments, which leads to the charge localization. We note that these configurations have been considered to be of significant importance for the three-center, four-electron bonding in phase-change memory materials,<sup>[40]</sup> while recently, the occurrence of such sites in amorphous chalcogenide materials was discussed in terms of hyperbonding.<sup>[41]</sup>

Moreover, the calculations show that localization of one and/or two electrons and holes at the same intrinsic atomic environment inside the amorphous structure can result in weakening and potential breaking of these axial, highly polarizable, long bonds in the defective-octahedral configurations, which also can lead to bond switching with a nearby atom in the vicinity of the host defect environment. Hence, these observations suggest that electron and hole trapping could cause athermal bond breaking within the amorphous network of the chalcogenide materials.

This study reinforces the evidence of electron/hole trapping in the narrow bandgap of the glassy chalcogenide structures, as we suggested previously in amorphous phase-change memory materials. The results presented here strengthen the observations reported in our previous work, regarding the energy levels of the charge-trapping defects in the bandgaps of the modeled structures, some of the atomic environments that host the electron/hole traps inside the glassy structures, and a potential bond-breaking pathway within the amorphous networks, while broadening the scope of the survey to more Ge-Sb-Te compositions, as well as to larger amorphous models (in an effort to eliminate system-size effects).

We note that a statistical analysis, through the examination of many (and ideally also larger) different amorphous models for each composition studied here (as well as for other compositions along the pseudo-binary tie-line), would be necessary to statistically predict the defect-state configurations, to investigate the probability of defect formation, and to gain a coherent picture of the atomic environments that are associated with the electron and hole traps within the various Ge-Sb-Te networks in the glassy state of phase-change memory materials, as we demonstrated in our previous work.<sup>[24,27]</sup>

In addition, electron trapping in the recrystallized state of phase-change memory materials should be studied in future investigations, since recently it was highlighted that spatially-localized electronic states are present at the bottom of the conduction band in recrystallized models of Ge<sub>2</sub>Sb<sub>2</sub>Te<sub>5</sub>,<sup>[42]</sup> and Ge<sub>1</sub>Sb<sub>2</sub>Te<sub>4</sub>,<sup>[43]</sup> associated with Te-Te homopolar bonds (i.e., Te anti-site defects) and Sb-Te chain structures.<sup>[42,43]</sup>

In conclusion, the current study corresponds to one step forward in the effort to build a comprehensive theoretical view about localized defect-related states in amorphous phase-change memory (and generally in glassy chalcogenide) materials. The suggested work earlier will give the opportunity to trace the defects holistically and to derive a universal mechanism for electron/hole trapping in Ge-Sb-Te phase-change memory materials.

## 7. Experimental Section

**Computer Models:** Details about the generated melt-quenched amorphous models used in this study to simulate charge trapping can be found in the previous works as follows: GeTe (180 atoms, DFT-MD),<sup>[28]</sup> Sb<sub>2</sub>Te<sub>3</sub> (250 atoms, DFT-MD),<sup>[31,34]</sup> Ge<sub>2</sub>Sb<sub>2</sub>Te<sub>5</sub> (900 atoms, GAP-MD),<sup>[27,44]</sup> and GeTe<sub>4</sub> (315 atoms, DFT-MD).<sup>[38]</sup>

**Modeling Charge Trapping:** Electron- and hole-trapping events were modeled by injecting an extra electron and hole, respectively, in the relaxed ground-state structure of each glass composition studied here, and then minimizing the energy with respect to the atomic coordinates. In each case, a homogeneous compensating background charge with opposite sign was applied in the simulation cell (positive/negative background charge for extra electron/hole). Double-charge trapping was also investigated by adding a second electron to the existing single-electron trapped model structures and then reoptimizing their geometries.

**Electronic-Structure Calculations:** Density-functional theory (DFT), as implemented in the CP2K code,<sup>[45]</sup> was used to optimize the geometries of the simulated glassy structures, and to calculate their electronic properties. The CP2K code employs a mixed Gaussian basis set with an auxiliary plane-wave basis set to represent the electrons in the modeled system.<sup>[46]</sup> A double- $\zeta$  valence-polarized (DZVP) Gaussian basis set was used for all atomic species (Ge, Sb, and Te),<sup>[47]</sup> in conjunction with the Goedecker–Teter–Hutter (GTH) pseudopotential.<sup>[48]</sup> The plane-wave energy cut-off was set to 5440 eV (400 Ry). The range-separated hybrid PBE0 functional was used in all the calculations.<sup>[49]</sup> The amount of exact exchange and the cut-off radius of this hybrid functional can be adjusted to achieve optimal accuracy for the electronic structure of the particular system under study.<sup>[21,24,27,42,50–53]</sup> Here, starting from the default values for PBE0, the cut-off radius was tuned, as a variational parameter, to minimize a deviation of the functional from straight-line behavior (see also Ref.[54] for details). Hence, in this work, an amount of 25% for the Hartree–Fock exchange, with cut-off radii of 2, 3, and 5.5 Å for the truncated Coulomb operator, were employed for Sb<sub>2</sub>Te<sub>3</sub>, GeTe and Ge<sub>2</sub>Sb<sub>2</sub>Te<sub>5</sub>, and GeTe<sub>4</sub>, respectively. The inclusion of the Hartree–Fock exchange with such parametrizations provided a more reliable description of the bandgaps and the localized defect electronic states that were potentially present in each of our glass models and which were involved in charge-trapping events. The computational cost of hybrid-functional calculations was reduced by using the auxiliary density-matrix method (ADMM),<sup>[55]</sup> as successfully employed in previous modeling studies of amorphous materials.<sup>[56,57]</sup> The Broyden–Fletcher–Goldfarb–Shanno (BFGS) algorithm was applied in the geometry optimizations of the amorphous structures to minimize the total energy of the modeled systems. The convergence criterion for the forces on atoms of the current configuration in an iteration step was 0.023 eV Å<sup>-1</sup> ( $4.5 \times 10^{-4}$  Hartree Bohr<sup>-1</sup>). Periodic-boundary conditions were enforced in all the calculations.

## Supporting Information

Supporting Information is available from the Wiley Online Library or from the author.

## Acknowledgements

The work has been performed under the Project HPC-EUROPA3 (INFRAIA-2016-1-730897), with the support of the EC Research Innovation Action under the H2020 Programme; in particular, K.K. gratefully acknowledges the computer resources and technical support provided by the Barcelona Supercomputing Center (BSC). K.K. acknowledges financial support from the Academy of Finland project No. 322832 “NANOIONICS”. The authors wish to acknowledge the CSC–IT Center for Science, Finland, for computational resources. The authors thank Dr T. H. Lee for providing the amorphous models of GeTe and GeTe<sub>4</sub>. The authors thank Dr J. Mavračić for providing the amorphous model of Sb<sub>2</sub>Te<sub>3</sub>.

## Conflict of Interest

The authors declare no conflict of interest.

## Data Availability Statement

The data that support the findings of this study are available from the corresponding author upon reasonable request.

## Keywords

amorphous chalcogenide materials, defect electronic states, electronic structures, electron trapping, hole trapping, phase-change memory

Received: December 17, 2022

Revised: March 1, 2023

Published online: April 24, 2023

- [1] S. Raoux, W. Welnic, D. Ielmini, *Chem. Rev.* **2010**, *110*, 240.
- [2] P. Noé, C. Vallée, F. Hippert, F. Fillot, J. Y. Raty, *Semicond. Sci. Technol.* **2018**, *33*, 013002.
- [3] R. Bez, A. Pirovano, *Mater. Sci. Semicond. Process.* **2004**, *7*, 349.
- [4] C. Longeaud, J. Luckas, D. Krebs, R. Carius, J. Klomfass, M. Wuttig, *J. Appl. Phys.* **2012**, *112*, 113714.
- [5] J. Luckas, D. Krebs, S. Grothe, J. Klomfass, R. Carius, C. Longeaud, M. Wuttig, *J. Mater. Res.* **2013**, *28*, 1139.
- [6] M. Kaes, M. Salinga, *Sci. Rep.* **2016**, *6*, 31699.
- [7] A. Pirovano, A. L. Lacaita, F. Pellizzer, S. A. Kostylev, A. Benvenuti, R. Bez, *IEEE Trans. Electron. Dev.* **2004**, *51*, 714.
- [8] B. Huang, J. Robertson, *Phys. Rev. B* **2012**, *85*, 125305.
- [9] D. Ielmini, Y. Zhang, *J. Appl. Phys.* **2007**, *102*, 054517.
- [10] A. Redaelli, A. Pirovano, A. Benvenuti, A. L. Lacaita, *J. Appl. Phys.* **2008**, *103*, 111101.
- [11] D. Krebs, R. M. Schmidt, J. Klomfass, J. Luckas, G. Bruns, C. Schlockermann, M. Salinga, R. Carius, M. Wuttig, *J. Non-Cryst. Solids* **2012**, *358*, 2412.
- [12] D. Ielmini, S. Lavizzari, D. Sharma, A. L. Lacaita, *Appl. Phys. Lett.* **2008**, *92*, 193511.
- [13] D. Ielmini, M. Boniardi, A. L. Lacaita, A. Redaelli, A. Pirovano, *Microelectron. Eng.* **2009**, *86*, 1942.
- [14] M. Boniardi, D. Ielmini, *Appl. Phys. Lett.* **2011**, *98*, 243506.
- [15] M. Wimmer, M. Kaes, C. Dellen, M. Salinga, *Front. Phys.* **2014**, *2*, 75.
- [16] J. Y. Raty, W. Zhang, J. Luckas, C. Chen, R. Mazzarello, C. Bichara, M. Wuttig, *Nat. Commun.* **2015**, *6*, 7467.
- [17] S. Gabardi, S. Caravati, G. C. Sosso, J. Behler, M. Bernasconi, *Phys. Rev. B* **2015**, *92*, 054201.
- [18] F. Zipoli, D. Krebs, A. Curioni, *Phys. Rev. B* **2016**, *93*, 115201.
- [19] M. Le Gallo, D. Krebs, F. Zipoli, M. Salinga, A. Sebastian, *Adv. Electron. Mater.* **2018**, *4*, 1700627.
- [20] B. Kersting, S. Ghazi Sarwat, M. Le Gallo, K. Brew, S. Walfort, N. Saulnier, M. Salinga, A. Sebastian, *Adv. Funct. Mater.* **2021**, *31*, 2104422.
- [21] K. Konstantinou, F. C. Mocanu, J. Akola, S. R. Elliott, *Acta Mater.* **2022**, *223*, 117465.
- [22] R. S. Khan, F. Dirisaglik, A. Gokirmak, H. Silva, *Appl. Phys. Lett.* **2020**, *116*, 253501.
- [23] S. R. Elliott, *J. Phys. D: Appl. Phys.* **2020**, *53*, 214002.
- [24] K. Konstantinou, S. R. Elliott, J. Akola, *J. Mater. Chem. C* **2022**, *10*, 6744.
- [25] H. Li, J. Robertson, *Appl. Phys. Lett.* **2020**, *116*, 052103.
- [26] S. Caravati, M. Bernasconi, T. D. Kühne, M. Krack, M. Parrinello, *J. Phys.: Condens. Matter.* **2009**, *21*, 255501.
- [27] K. Konstantinou, F. C. Mocanu, T. H. Lee, S. R. Elliott, *Nat. Commun.* **2019**, *10*, 3065.
- [28] T. H. Lee, S. R. Elliott, *Adv. Mater.* **2020**, *32*, 2000340.
- [29] J. W. Park, S. H. Eom, H. Lee, J. L. F. Da Silva, Y. S. Kang, T. Y. Lee, Y. H. Khang, *Phys. Rev. B* **2009**, *80*, 115209.
- [30] D. Krebs, S. Raoux, C. T. Rettner, G. W. Burr, M. Salinga, M. Wuttig, *Appl. Phys. Lett.* **2009**, *95*, 082101.
- [31] K. Konstantinou, J. Mavračić, F. C. Mocanu, S. R. Elliott, *Phys. Status Solidi B* **2021**, *258*, 2000416.
- [32] S. Caravati, M. Bernasconi, M. Parrinello, *Phys. Rev. B* **2010**, *81*, 014201.
- [33] J. K. Olson, H. Li, T. Ju, J. M. Viner, P. C. Taylor, *J. Appl. Phys.* **2006**, *99*, 103508.
- [34] F. C. Mocanu, K. Konstantinou, J. Mavračić, S. R. Elliott, *Phys. Status Solidi RRL* **2021**, *15*, 2000485.
- [35] F. C. Mocanu, K. Konstantinou, T. H. Lee, N. Bernstein, V. L. Deringer, G. Csányi, S. R. Elliott, *J. Phys. Chem. B* **2018**, *122*, 8998.
- [36] J. Akola, R. O. Jones, *Phys. Rev. B* **2007**, *76*, 235201.
- [37] J. Hegedüs, S. R. Elliott, *Nat. Mater.* **2008**, *7*, 399.
- [38] M. A. Hughes, Y. Fedorenko, B. Gholipour, J. Yao, T. H. Lee, R. M. Gwilliam, K. P. Homewood, S. Hinder, D. W. Hewak, S. R. Elliott, R. J. Curry, *Nat. Commun.* **2014**, *5*, 5346.
- [39] P. Petkov, M. Wuttig, P. Ilchev, T. Petkova, *J. Optoelectron. Adv. Mater.* **2003**, *5*, 1101.
- [40] A. V. Kolobov, P. Fons, J. Tominaga, S. R. Ovshinsky, *Phys. Rev. B* **2013**, *87*, 165206.
- [41] T. H. Lee, S. R. Elliott, *Nat. Commun.* **2022**, *13*, 1458.
- [42] K. Konstantinou, F. C. Mocanu, J. Akola, *Phys. Rev. B* **2022**, *106*, 184103.
- [43] Y. Xu, Y. Zhou, X. D. Wang, W. Zhang, E. Ma, V. L. Deringer, R. Mazzarello, *Adv. Mater.* **2022**, *34*, 2109139.
- [44] F. C. Mocanu, K. Konstantinou, S. R. Elliott, *J. Phys. D: Appl. Phys.* **2020**, *53*, 244002.
- [45] J. VandeVondele, M. Krack, F. Mohamed, M. Parrinello, T. Chassaing, J. Hutter, *Comput. Phys. Commun.* **2005**, *167*, 103.
- [46] G. Lippert, J. Hutter, M. Parrinello, *Mol. Phys.* **1997**, *92*, 477.
- [47] J. VandeVondele, J. Hutter, *J. Chem. Phys.* **2007**, *127*, 114105.
- [48] S. Goedecker, M. Teter, J. Hutter, *Phys. Rev. B* **1996**, *54*, 1703.
- [49] M. Guidon, J. Hutter, J. VandeVondele, *J. Chem. Theory Comput.* **2009**, *5*, 3010.
- [50] O. A. Dicks, A. L. Shluger, *J. Phys.: Condens. Matter* **2017**, *29*, 314005.
- [51] J. Strand, M. Kaviani, D. Gao, A. M. El-Sayed, V. V. Afanas'ev, A. L. Shluger, *J. Phys.: Condens. Matter* **2018**, *30*, 233001.
- [52] K. Konstantinou, T. H. Lee, F. C. Mocanu, S. R. Elliott, *Proc. Natl. Acad. Sci. USA* **2018**, *115*, 5353.
- [53] D. Mora-Fonz, M. Kaviani, A. L. Shluger, *Phys. Rev. B* **2020**, *102*, 054205.
- [54] A. Karolewski, L. Kronik, S. Kümmel, *J. Chem. Phys.* **2013**, *138*, 204115.
- [55] M. Guidon, J. Hutter, J. VandeVondele, *J. Chem. Theory Comput.* **2010**, *6*, 2348.
- [56] A. M. El-Sayed, M. B. Watkins, V. V. Afanas'ev, A. L. Shluger, *Phys. Rev. B* **2014**, *89*, 125201.
- [57] K. Konstantinou, D. M. Duffy, A. L. Shluger, *Phys. Rev. B* **2016**, *94*, 174202.